Asymmetric Catalysis

Cooperative Lewis Acid-1,2,3-Triazolium-Aryloxide Catalysis: Pyrazolone Addition to Nitroolefins as Entry to Diaminoamides

Daniel M. Wanner[+], Patrick M. Becker[+], Simon Suhr, Nick Wannenmacher, Slava Ziegler, Justin Herrmann, Felix Willig, Julia Gabler[†], Khushbu Jangid, Juliane Schmid, Andreas C. Hans, Wolfgang Frey, Biprajit Sarkar, Johannes Kästner, and René Peters*

In memory of Julia Gabler

Abstract: Pyrazolones represent an important structural motif in active pharmaceutical ingredients. Their asymmetric synthesis is thus widely studied. Still, a generally highly enantio- and diastereoselective 1,4-addition to nitroolefins providing products with adjacent stereocenters is elusive. In this article, a new polyfunctional Cu^{II}-1,2,3-triazolium-aryloxide catalyst is presented which enables this reaction type with high stereocontrol. DFT studies revealed that the triazolium stabilizes the transition state by hydrogen bonding between C(5)–H and the nitroolefin and verify a cooperative mode of activation. Moreover, they show that the catalyst adopts a rigid chiral cage/pore structure by intramolecular hydrogen bonding, by which stereocontrol is achieved. Control catalyst systems confirm the crucial role of the triazolium, aryloxide and Cu^{II}, requiring a sophisticated structural orchestration for high efficiency. The addition products were used to form pyrazolidinones by chemoselective C=N reduction. These heterocycles are shown to be valuable precursors toward β,γ'-diaminoamides by chemoselective nitro and N–N bond reductions. Morphological profiling using the Cell painting assay identified biological activities for the pyrazolidinones and suggest modulation of DNA synthesis as a potential mode of action. One product showed biological similarity to Camptothecin, a lead structure for cancer therapy.

Introduction

Chiral β-aminoamides build a compound class of large medicinal importance.[1] There are numerous commercialized drugs of this type for the treatment of various diseases. Prominent examples include, e.g., Knyostatin (KNI-272) as HIV protease inhibitor,[2] Sitagliptin for the treatment of type II diabetes[3] and Bestatin as anticancer agent (Scheme 1).[4] Also achiral β-aminoamides such as the local anesthetic Lidocaine (Scheme 1) are medicinally important.[4]

Different strategies have been reported for the catalytic asymmetric synthesis of β-aminoamides.[1a,5] The most common ones rely on Mannich additions,[1a,6] reductive aminations,[7,1a] enamine reductions,[8] aza-Michael additions[9] and enzyme catalyzed resolutions.[10] An access to chiral enantioenriched β-aminoamides starting from pyrazolones is underdeveloped. Recently we reported the

[*]   Dr. D. M. Wanner,[+] Dr. N. Wannenmacher, J. Herrmann,
      Dr. F. Willig, J. Gabler, K. Jangid, Dr. J. Schmid, A. C. Hans,
      Dr. W. Frey, Prof. Dr. R. Peters
      Universität Stuttgart, Institut für Organische Chemie
      Pfaffenwaldring 55, 70569 Stuttgart (Germany)
      E-mail: rene.peters@oc.uni-stuttgart.de

      P. M. Becker,[+] Prof. Dr. J. Kästner
      Universität Stuttgart, Institut für Theoretische Chemie
      Pfaffenwaldring 55, 70569 Stuttgart (Germany)

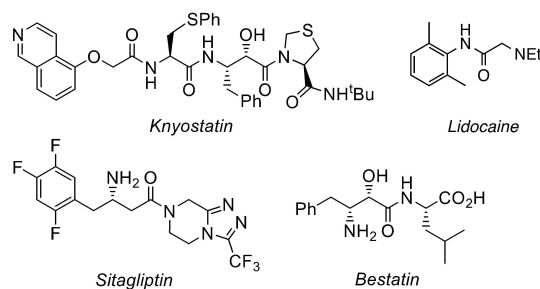   S. Suhr, Prof. Dr. B. Sarkar
      Universität Stuttgart, Institut für Anorganische Chemie
      Pfaffenwaldring 55, 70569 Stuttgart (Germany)

      Dr. S. Ziegler
      Max Planck Institute of Molecular Physiology, Department of
      Chemical Biology
      Otto-Hahn-Strasse 11, 44227 Dortmund (Germany)

[+]   These authors contributed equally to this work.

[†]   deceased in January 2023

Scheme 1. Examples for prominent β-aminoamide drugs.

only currently known example using a 4,4-dialkyl substituted pyrazolone.[11]

Pyrazolones in their own right also feature remarkable biological properties[12] and are important for medical use.[13,14] For instance, they act as tumor cell inhibitors,[15] and are studied in rheumatism therapy as tumor necrosis factor (TNF) inhibitors.[16] Important drugs are, e.g., Edaravon[13a,17] to treat both ALS (amyotrophic lateral sclerosis, a neurodegenerative disease) and acute ischemic stroke, and Antipyrin as a non-opioid analgesic.[12a]
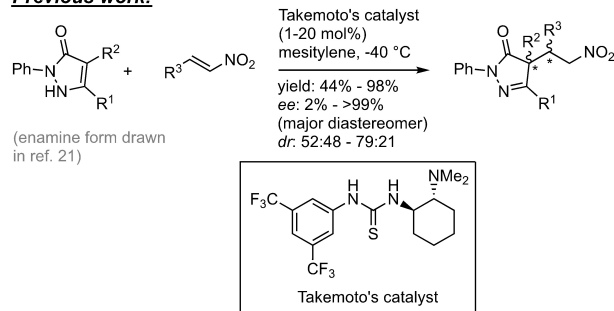
Due to the significance of pyrazolones in medicine and many other fields,[18] their synthesis and functionalization has been extensively studied.[19] An obvious option for asymmetric synthesis is based on the C,H acidity of the 4-position,[19a,c] which was employed in various 1,4-additions.[20] Nevertheless, so far a single method is known for the catalytic enantioselective 1,4-addition to nitroolefins, by which adjacent stereocenters are simultaneously formed at the pyrazolone and the Michael acceptor (Scheme 2, *top*).[21,22] Yuan et al. reported that high to excellent enantioselectivity was attained with Takemoto's catalyst[23] for one pyrazolone with a large number of different nitroolefins.[21] For the other three reactive pyrazolones investigated, the reaction outcomes were strongly dependent on their substitution patterns. Enantiomeric excesses (ee's) varied from 2% to >99%. The products were formed with low to moderate diastereoselectivity (diastereomeric ratios (dr's) up to 79:21), but mostly with excellent yields. In all other reported methods, C(4)-unsubstituted pyrazolones were used, providing aromatic tautomers as products (i.e. no stereocenter at the pyrazolone is formed).[24]

Herein, we report that a new polyfunctional Lewis acid-1,2,3-*triazolium*-aryloxide catalyst enables the asymmetric 1,4-addition of C(4)-substituted pyrazolones to nitroolefins with excellent scope, high enantioselectivity and yields and usually good to high diastereoselectivity (dr up to 99:1, Scheme 2, middle).[25] We showcase that the products lead to pyrazolidinones and β,γ'-diaminoamides. For the pyrazolidinones, morphological profiling identified biologically active derivatives, in particular biosimilarity to the anticancer agent Camptothecin.[26]
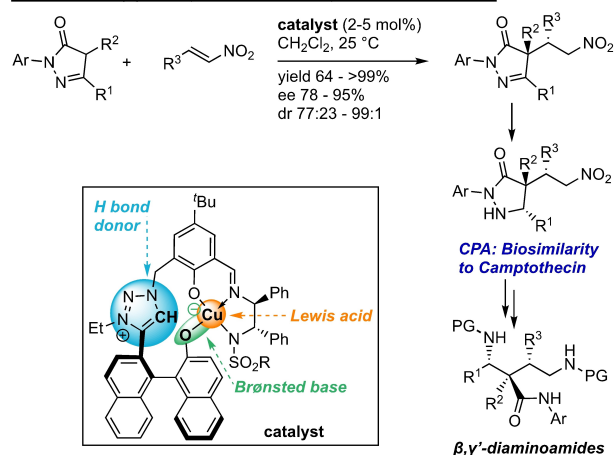
Prior to this study we reported Lewis acid-*imidazolium*-aryloxides to be very effective cooperative polyfunctional catalysts in asymmetric 1,4-additions of β-ketoesters[27] and [4+2]-cycloadditions of C,H acidic prodienes.[28] As density functional theory (DFT) studies revealed, in these systems the imidazolium unit stabilizes the transition state by hydrogen bonding between the H at C(2) and the electron poor olefin.[27]

Since we found in the present study that this previous catalyst type showed a moderate performance in the title reaction, the corresponding 1,2,3-*triazolium* catalysts were studied here. From materials science it is known that the H atoms at C(5) of a 1,2,3-triazolium unit are more efficient H bond donors, with a strength comparable to secondary amides.[29,30] DFT studies confirm the postulated cooperative mode of activation.[31,32] They show that the catalyst forms a rigid chiral pocket by intramolecular H-bonding between the naphthol OH (formed after proton transfer from the
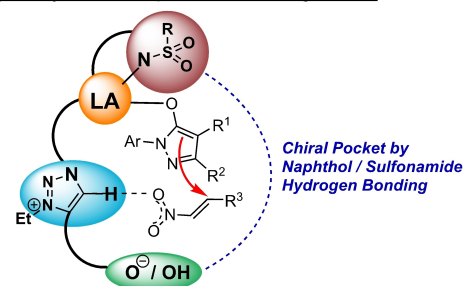
Previous work:

(enamine form drawn in ref. 21)

Takemoto's catalyst (1-20 mol%) mesitylene, -40 °C
yield: 44% - 98%
ee: 2% - >99% (major diastereomer)
dr: 52:48 - 79:21

Takemoto's catalyst

This work: (a) catalyst design and synthetic application

catalyst (2-5 mol%) CH₂Cl₂, 25 °C
yield 64 - >99%
ee 78 - 95%
dr 77:23 - 99:1

CPA: Biosimilarity to Camptothecin

β,γ'-diaminoamides

catalyst

(b) catalyst modus operandi according to DFT

Chiral Pocket by Naphthol / Sulfonamide Hydrogen Bonding

Scheme 2. Comparison of previous work to this work, new catalyst design and modus operandi plus synthetic applications.
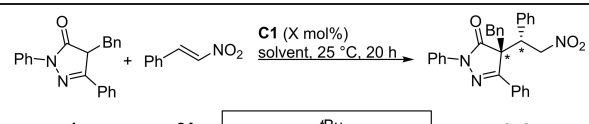
coordinated pronucleophile to the naphthoxide) and one sulfonamide O atom of the ligand, by which stereocontrol is enabled (Scheme 2, bottom).

Results and Discussion

Optimization

Catalyst **C1** with a 1,2,3-triazolium moiety was studied in the addition of pyrazolone **1a** to **2A** as model reaction (Table 1).

For the model reaction several solvents were initially screened at 25 °C using 5 mol% of **C1** (entries 1–4). Chlorinated solvents were well suited, whereas Lewis basic solvents like THF (tetrahydrofuran) and MeCN resulted in

Table 1: Optimization of the model reaction.

| #	X mol% C1	solvent	conc. (mol/L)[a]	conv. (%)[a]	yield (%)[a]	dr[b]	ee (%)[c]
1	5	THF	0.2	90	90	91:9	74
2	5	MeCN	0.2	80	80	83:17	34
3	5	(CH2Cl)2	0.2	96	92	90:10	88
4	5	CH2Cl2	0.2	99	99	93:7	93
5	2	CH2Cl2	0.2	78	78	93:7	91
6	2	CH2Cl2	0.1	60	60	96:4	94
7[d]	2	CH2Cl2	0.1	90	90	91:9	91
8[d,e]	2	CH2Cl2	0.1	94	94	95:5	94

[a] Determined by ^{1}H NMR using an internal standard. [b] Diastereomeric ratio determined by ^{1}H NMR. [c] Enantiomeric excess of the major diastereomer determined by HPLC. [d] Reaction time 48 h. [e] 1.1 equiv. of **1a** used.

lower enantioselectivity. By ^{1}H NMR we found that the keto tautomer of the substrate is strongly dominating in dichloromethane, in which the product was formed in nearly quantitative yield with a good dr and high ee (entry 4). Solvent degassing was important to avoid pyrazolone dimerization.

By reducing the catalyst loading to 2 mol% a lower yield was obtained (entry 5). At lower concentrations the product yield further decreased, whereas the stereoselectivity could be improved (dr=96:4, ee=94%, entry 6). In both cases no side products were detected, but unreacted pyrazolone. To form the product in high yield the reaction time was increased to 48 h. The optimized conditions gave the product in 94% yield with a dr of 95:5 and an ee of 94% (entry 8). No side products were found.

Catalyst Synthesis

Catalyst **C1** is readily prepared in high yield from the known axially chiral building block **5** (Scheme 3),[33] derived from (R)-BINOL (1,1′-bi-2-naphthol), and the known benzylic azide **4**,[34] which is obtained from *p-tert.*-butylphenol (see Supporting Information). Both fragments were coupled via a Cu catalyzed azide/alkyne cycloaddition.[34] Subsequently, the methoxy group was demethylated by BBr$_3$.[33] The triazole ring was then N-alkylated by [Et$_3$O]PF$_6$ and imine **L1** was formed by condensation with an enantiopure aminosulfonamide. Complexation with Cu(acac)$_2$ was achieved in the presence of molecular sieves. The activated catalyst was
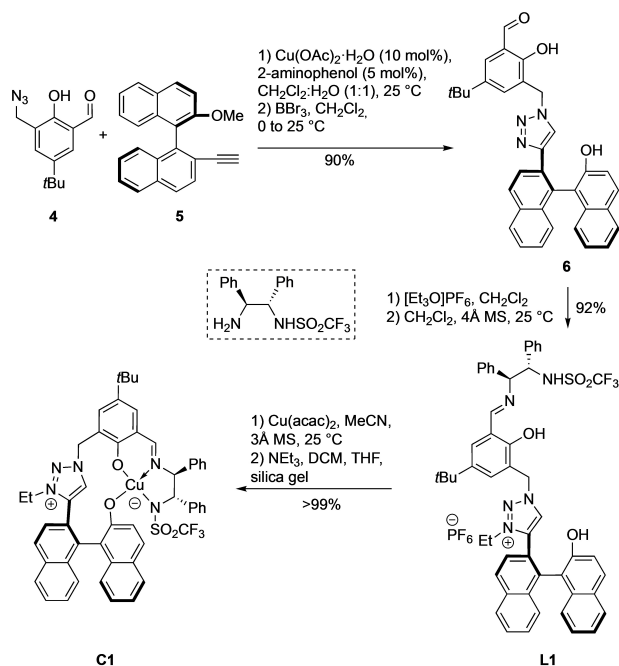
Scheme 3. Synthesis of catalyst **C1**.

obtained by filtration over silica gel in the presence of NEt$_3$. It was found to be stable for several months when stored at room temperature under N$_2$ atmosphere. The overall yield was 83% for the depicted sequence. The ligand structure was further confirmed by X-ray crystal structure analysis of a closely related derivative **L1-Br** carrying a Br atom rather than the *t*Bu group at the phenol ring (Figure 1).[35]

Scope

The model reaction was then performed on a 1.0 mmol scale under the conditions of Table 1/entry 9. **3bA** was produced in 94% yield (0.489 g) with an ee of 94% and a dr of 94:6 (Table 2, entry 2). Other benzylic residues like 2-naphthylmethyl were also well tolerated (entry 3) providing high dr values. Also alkyl residues R^1 can be used as exemplified in entries 4 and 5 for CH$_3$ and CH$_2$CH$_2$OH,
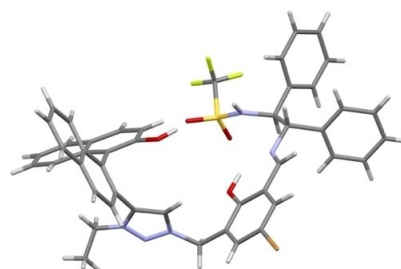

Figure 1. X-ray crystal structure analysis of **L1-Br**. White: H, gray: C, red: O, blue: N, yellow: S, green: F, brown: Br. PF$_6^-$ and solvent molecules are not shown for clarity.[35]

Table 2: Investigation of the pyrazolone scope.

#	R^1	R^2	R	3	yield (%)[a]	dr[b]	ee (%)[c]
1	Bn	Ph	Ph	3aA	94	95:5	94
2	p-Me-C$_6$H$_4$	Ph	Ph	3bA	99	94:6	94
3	CH$_2$-2-Naph	Ph	Ph	3cA	80	96:4	91
4	Me	Ph	Ph	3dA	80	89:11	90
5[e]	(CH$_2$)$_2$OH	Ph	Ph	3eA	99	84:16	80
6	CH$_2$-CCH	Ph	Ph	3fA	90	93:7	95
7	CH$_2$-CH=CH$_2$	Ph	Ph	3gA	95	86:14	93
8[e]	F	Ph	Ph	3hA	78	93:7	90
9	Bn	Me	Ph	3iA	80	77:23	86
10[f]	Bn	iPr	Ph	3jA	78	82:18	78
11	Bn	Ph	PMP	3kA	80	90:10	91
12	Bn	Ph	Bn	3lA	64	86:14	81
13	Bn	Ph	m-Cl-C$_6$H$_4$	3mA	94	94:6	90

[a] Yield of isolated product. [b] Diastereomeric ratio determined by ^{1}H NMR of the crude product. [c] Enantiomeric excess of the major diastereomer determined by HPLC. [d] 4 mol% catalyst, $c = 0.2$ M. [e] 5 mol% catalyst, $c = 0.2$ M, reaction time 20 h. [f] 5 mol% catalyst, $c = 0.2$ M, reaction time 3 d.

Table 3: Investigation of the nitroolefin scope.

#	X	R^3	3	yield (%)[a]	dr[b]	ee (%)[c]
1	2	p-Me-C$_6$H$_4$	3aB	99	97:3	91
2	3	m-Me-C$_6$H$_4$	3aC	93	93:7	92
3	2	p-Br-C$_6$H$_4$	3aD	89	96:4	95
4	3	m-Br-C$_6$H$_4$	3aE	99	90:10	90
5	2	p-MeO-C$_6$H$_4$	3aF	96	95:5	90
6	4	m-MeO-C$_6$H$_4$	3aG	99	95:5	93
7	4	o-MeO-C$_6$H$_4$	3aH	80	93:7	85
8	2	(benzodioxole)	3aI	73	95:5	85
9	2	p-O$_2$N-C$_6$H$_4$	3aJ	98	91:9	74
10	2	2-naphthyl	3aK	78	96:4	92
11	2	2-furanyl	3aL	99	98:2	85
12	2	2-thienyl	3aM	83	96:4	85
13	5	cyclopropyl	3aN	>99	99:1	92
14	5	^{i}Pr	3aO	70	95:5	87
15	5	^{i}Bu	3aP	65	93:7	87

[a] Yield of isolated product. [b] Diastereomeric ratio determined by ^{1}H NMR of the crude product. [c] Enantiomeric excess of the major diastereomer determined by HPLC.

respectively. The hydroxy moiety did not have to be protected.

In addition, propargyl and allyl residues R^1 were well accommodated (entries 6&7). Particularly interesting is entry 8, in which the pyrazolone carries a F atom at C(4). Still, the product was formed in good yield with high diastereo- and enantioselectivity.[36]

Moreover, the impact of the residues R^2 was examined. With aliphatic ones the reaction provided good yields and stereoselectivity was moderate to good (entries 9&10). Synthetically important is the fact that for the first time N-substituents R could also be employed that might serve as a removable protective group, namely *para*-methoxyphenyl (PMP, entry 11) and benzyl (entry 12).

The 1,4-addition was also applied to a number of different nitroolefins 2 (Table 3). Apparently, the electronic influence of substituent R^3 is relatively small, as substrates equipped with σ-donors (Me, entries 1&2), σ-acceptors (Br, *m*-OMe, entries 3, 4, 6&8) and π-donors (*o*-&*p*-OR, entries 5, 7&8) all provided similar results. Also, with a π-acceptor substituent (*p*-NO$_2$, entry 9), a nearly quantitative yield was attained, but ee was lower.

R^3 = 2-naphthyl was used as an example for an extended π-system (entry 10) and 2-furanyl as well as 2-thienyl as electron rich heterocycles (entries 11&12). Yields were high in all cases.

In general, diastereomeric ratios were in each case significantly higher than in literature,[21] ranging from 77:23 (Table 2, entry 4) to 99:1 (Table 3, entry 13). Ee values were good to high in all cases, ranging from 74 to 95%. Even alkyl substituted nitroolefins worked fine despite their

C–H acidity (entries 13–15). These 28 examples demonstrate the synthetic value of the title reaction.

To study if the catalyst might be reused, it was isolated by filtration over silica gel after the catalytic reaction, which proceeded in quantitative yield. As the naphtholate is protonated by silica gel, the catalyst sticked on the top of the filter cake while product was eluted. Then the silica pad was treated with THF/CH$_2$Cl$_2$/NEt$_3$ (66:33:1) to regenerate the active catalyst, which was recovered in pure form as confirmed by ESI-MS and UV/Vis. In the second run, stereoselectivity was again on a high level (Scheme 4).

Mechanistic Studies and Considerations

a) Control Systems

To elucidate which functional groups of the polyfunctional catalyst are essential for a high catalytic efficiency, a number of control catalysts was studied (Table 4).

For comparison, entry 1 shows the result of the model reaction with standard catalyst **C1**. Formally changing the
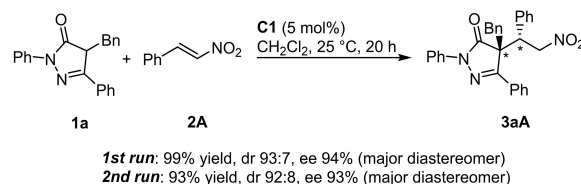

1st run: 99% yield, dr 93:7, ee 94% (major diastereomer)
2nd run: 93% yield, dr 92:8, ee 93% (major diastereomer)

Scheme 4. Reusing catalyst **C1**.

Table 4: Experiments with control catalysts.

#	catalyst	yield (%)[a]	dr[b]	ee (%)[c]
1	**C1**	99	93:7	93
2	**C2**	98	90:10	78
3	**C3**	<2	69:31	n.d.
4	**C4** + Na(acac) (2.5 mol%)	84	82:18	−10
5	**C5**	65	87:13	−4
6	**C6**	86	90:10	−5
7	**C7**	99	93:7	16
8	**C8** + Na(acac) (2.5 mol%)	27	81:19	48
9	**C9** + **C10**	75	59:41	rac.
10	**C10**	23	56:44	rac.
11	**C10** + Cu(OTf)₂ (5 mol%)	3	51:49	n.d.

[a] Determined by ^{1}H NMR using mesitylene as internal standard. [b] Diastereomeric ratio determined by ^{1}H NMR . [c] Enantiomeric excess of the major diastereomer determined by HPLC. A negative value indicates that the enantiomer not depicted was formed in excess.

triazolium unit of **C1** to an imidazolium unit in **C2** led to a significant decrease of the enantiomeric excess (entry 2), although the position of the C(2)–H bond of the imidazolium fragment is equivalent to the C(5)–H bond of the triazolium unit. We ascribe this to the stronger H-bond donor capacity of the triazolium ring.[29]

Formal O-methylation of **C1** to the corresponding methyl ether resulted in a nearly complete loss of reactivity (entry 3). This confirms the necessity of the basic unit.[37]

Control catalyst **C4** features a neutral triazole unit (entry 4). To this Cu complex Na(acac) (acac = acetylaceto-nate) was added to form the naphtholate unit. By this change enantioselectivity was largely lost, suggesting that a charged triazolium hydrogen bond donor is beneficial.

In catalyst **C5** and **C6** the element of axial chirality is missing (entries 5&6). The formation of nearly racemic product reveals that the binaphthyl fragment is crucial for stereocontrol. Calculations suggest that a rigid chiral cage formation is the reason for that (vide infra).

Entry 7 suggests that the higher flexibility in **C7** apparently has a negative influence on the enantioselectivity. The use of catalyst **C8** (plus Na(acac)) lacking an azolium moiety resulted in a poor yield and low stereoselectivity (entry 8).

A binary catalyst system consisting of **C9** featuring a simple methyl residue and betaine **C10** (both 5 mol%) resulted in racemic product with poor diastereoselectivity (entry 9). The use of just **C10** as catalyst also provided racemic product and activity was poor (entry 10). By addition of Cu(OTf)₂ as cocatalyst reactivity nearly vanished (entry 11).

These results demonstrate the necessity of a Lewis acid, the azolium and aryloxide units, but also that a polyfunctional catalyst system with a sophisticated structural orchestration is required for satisfying results in yield, diastereo- and enantioselectivity. An intramolecular cooperation of these functional groups is thus likely. Since we found a linear product ee dependence on the catalyst ee (see Supporting Information), the claim that only one catalyst molecule is involved in a catalytic cycle, is supported.[38]

b) Structural and Spectroscopic Studies

In agreement with this, it was found by UV/Vis studies (Beer's plot, see Supporting Information) that the activated catalyst is a monomeric species. By ESI-HRMS during the catalytic reaction, a complex of the pyrazolone and catalyst could be detected with the expected isotopic pattern (m/z calculated for $[C_{73}H_{62}CuF_3N_7O_5S + Na]^+$: 1291.3673, found: 1291.3679, see Supporting Information).

Due to their $S = ^1/_2$ spin state and a nuclear spin of $I = 3/2$, Cu^{II} systems are amenable to EPR spectroscopy and give characteristic signals that yield information on the coordination geometry. Both the non-activated and activated complex display axial EPR spectra in solution with $g_\parallel > g_\perp > g_{el}$, indicating a d_{x2-y2} ground state (see Figure S12). According to the Peisach-Blumberg maps, the complexes fall into the $[N_2O_2]X_2$ category.[39] $g_\parallel$-values of around 2.2 in combination with $A_\parallel$ values between 500 MHz ($167 \cdot 10^{-4}$ cm^{-1}) and 570 MHz ($190 \cdot 10^{-4}$ cm^{-1}) point to either an elongated octahedron or an elongated square-bipyramid with little equatorial distortion ($g_\parallel / A_\parallel \geq 130$ cm).[40] The sulfonamide may bind via one of its oxygen atoms and serve as an axial ligand. In order to get further mechanistic insights, we performed EPR studies on the interaction between the activated catalyst and the substrates. The addition of pyrazolone **1b** leads to a change in the EPR spectrum (Figure 2), most noticeable in the higher field region, and indicates binding of the substrate to the activated catalyst.
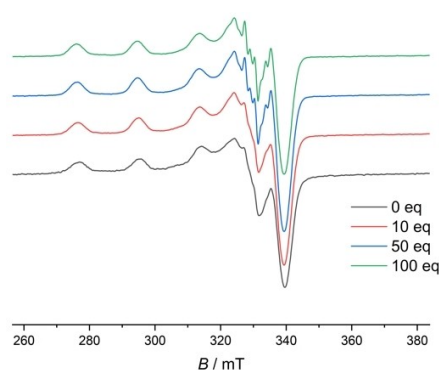
Figure 2. X-band EPR spectrum obtained after the addition of pyrazolone substrate to activated catalyst.

This observation is in accordance with the found mass of a pyrazolone-catalyst complex during the catalytic reaction, mentioned before.

Similar *g*-values in the activated catalyst before and after binding of the substrate points to structural similarities in both species. Full transformation of the spectrum is achieved after addition of 50 equiv. of pyrazolone. A similar trend is observed upon the addition of the catalytic product: changes in the spectrum become apparent in the presence of 10 equiv. of product (Figure S15).

c) Computational Studies

To further investigate structural properties of **C1** as well as to elucidate the mechanism of the catalytic reaction, we performed DFT calculations on the B3LYP-D3(BJ)/def2-TZVP/COSMO(DCM) level of theory on PBEh-3c-D3(BJ)/def2-mSVP geometries.[41] Since no crystal structure of **C1** is available, a model was built manually, based on calculated geometries of the imidazolium system **C2** (see Supporting Information).[27] This served as starting point for all further geometries.

The precatalyst (i.e., prior to activation by NEt$_3$) possesses two acidic H-atoms: one at the binaphthol moiety and one at the triazolium unit. We aimed to elucidate which site is deprotonated in the precatalyst. Three coordination sites of the Cu^{II} center are occupied by the nitrogen atoms of the iminosulfonamide backbone and the phenolate-O atom. A fourth one could either be filled with the aryloxide O-atom or a corresponding mesoionic carbene (MIC) carbon atom, resulting in a distorted square planar coordination of the Cu^{II} center.[42] According to our computational results, the binaphthol moiety is more acidic than the triazolium unit, which results in an energetic favor of the aryloxide complex relatively to the MIC complex by 74.2 kJ mol^{-1}. This finding agrees with the results of EPR spectroscopic studies of **C1** (vide supra), indicating an [N$_2$O$_2$]X$_2$ or [N$_2$O$_2$]X environment for the Cu center. In principle, the aryloxide O-atom could also coordinate in an intermolecular fashion forming a bimetallic complex like it was found by us for a Cu^{II}-imidazolium-phenolate catalyst in

the solid state.[28] The dimerization of **C1** is endergonic by 7.2 kJ mol^{-1} for the singlet and 16.0 kJ mol^{-1} for the triplet complex. Thus, **C1** is expected to be a monomeric species, which matches with the results of the UV/Vis studies (vide supra). Due to steric hindrance, it is possible to coordinate only one additional adduct partner (either THF, water, or NEt$_3$) at the Cu^{II} center in **C1**. These three adduct partners are present in the activation process of the catalyst. Because the adduct formation is only slightly exergonic for all those binding partners (except for NEt$_3$, for which endergonicity was found) and the fact that neither THF, nor water or NEt$_3$ should be present in the catalytic reaction mixture in significant quantities, we expect **C1** without any adduct partner (Figure 3) to be the catalytically active species. The structural chemistry of the related catalyst **C2** is similar (see Supporting Information).

Based on the described experimental and computational results, we propose a catalytic cycle, which is shown in Scheme 5.[43]

1a initially coordinates to **C1** by the keto forms **1a(R)** and **1a(S)**, since the enol tautomer was calculated to be 30.0 kJ mol^{-1} and the enamine 6.1 kJ mol^{-1} higher in energy. The formation of **C1-1a(R)** and **C1-1a(S)** is calculated to be exergonic by 19.9 kJ mol^{-1} and 14.7 kJ mol^{-1}, respectively.

The first step of the reaction cycle is a proton shift to the aryloxide, i.e., from **C1-1a** to **I**. Thereby, the local coordination environment of the Cu^{II} center does not change significantly, which agrees with EPR results (vide supra). The transition state energy for this reaction step with **C1-1a(R)** was found to be 42.4 kJ mol^{-1}. Deprotonated **1a** acts as a monodentate ligand in **I** implicating a significant conformational freedom. Its relative orientation at the catalyst is affected though by interaction with the surrounding by confinement effects. Our DFT results show a hydrogen bond between the binaphthol-OH and a sulfonamide oxygen evolving in a binding pocket arrangement in **I** creating a rigid chiral pore. Hydrogen bonding between the binaphthol-OH and a sulfonyl oxygen is also found for one of the energetically most favored conformers of the precatalyst (see Figure S36).
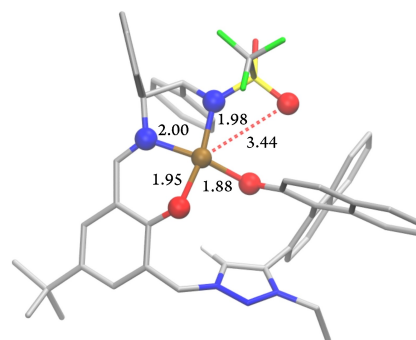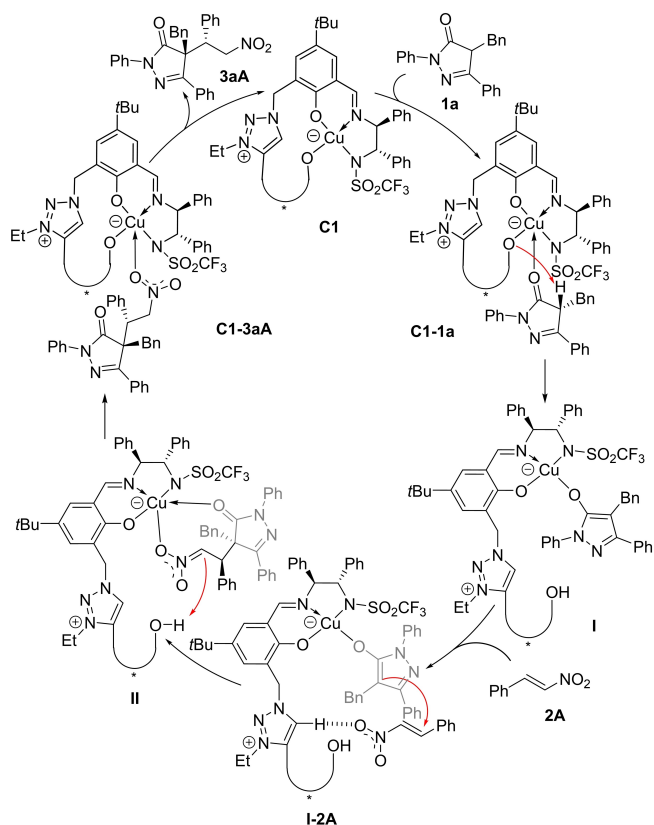

Figure 3. Most stable conformer of **C1**. Most hydrogen atoms are omitted for clarity, the Cu^{II} center and its local coordination environment are drawn as balls and specific bond lengths are shown in Å. White: H, gray: C, brown: Cu, red: O, blue: N, yellow: S, green: F.

Scheme 5. Proposed simplified catalytic cycle.

catalyst in this case seems to overcompensate the energy win caused by the double hydrogen bond activation of the nitroolefin.

The C–C bond formation, i.e., the step from **I-2A** to **II**, is stereodetermining. As two stereocenters are formed, in principle, four different configuration isomers must be considered. They differ in the nucleophile's and the nitro-olefin's orientation. We focus on the main product and its enantiomer. In Figure 4 the transition state structures for the C–C-bond formation step leading to (4*R*,1′*S*)- and (4*S*,1′*R*)-product configurations of **3aA** are compared.

The (4*R*,1′*S*)-transition state is stabilized by an interaction of the C(4) benzyl group with the π-system of the ligand's phenolate moiety. Due to this orientation the nucleophilic pyrazalone's C-atom is attacked by the nitro-olefin **2A** at the *Re*-side. A $\Delta\Delta G^0$ of 9.2 kJ mol^{-1} between the transition states (Figure 5) results in a predicted ee of 95 % for the (4*R*,1′*S*)-product, which agrees well with the results in Table 2. After C–C-bond formation, a subsequent intramolecular protonation of the nitronate intermediate leads to the product-catalyst-complex **C1-3aA** (for details of the protonation step see Supporting Information). According to our DFT results the transition state of this step is the rate determining transition state within the energetic span model (see Supporting Information). The dissociation of **C1-3aA** closes the catalytic cycle by re-forming **C1**. **C1-3aA** is energetically clearly disfavored compared to the substrate/catalyst complex **C1-1a**, by 12.0 kJ mol^{-1} for the main product and 6.7 kJ mol^{-1} for its enantiomer. That represents a significantly lower binding affinity of **3aA** towards the catalyst than **1a**.

As a next step, **2A** coordinates to **I**, forming **I-2A**. In all low-energy conformers we found of **I-2A** the nitroolefin is activated by a single hydrogen bond to the triazolium group's C(5)–H increasing the beta-C atom's electrophilic nature. Besides small geometric changes due to the triazolium/ imidazolium exchange, this finding supports the above-mentioned expectation of a stronger nitroolefin activation by the triazolium moiety in comparison to the imidazolium,[29] causing the higher activity and significantly better stereoselectivity of **C1** relative to **C2** (see Supporting Information). Additionally, the described single hydrogen bond activation modus distinguishes **C1** from other literature-known catalysts, e.g., Takemoto's catalyst, which are thought to act by a dual hydrogen bond-activation mode for nitroolefin electrophiles.[44] In combination with the enzyme-inspired arrangement of the catalyst due to the hydrogen bond between the binaphthol OH and sulfonamide this underlines the highly cooperative modus operandi of **C1**.

According to our initial mechanistic hypothesis, we expected two hydrogen bonds from the catalyst to the nitroolefin electrophile as described and discussed in section 9.10 from the Supporting Information. However, sampling of the conformational space (for the reactant, product, as well as transition state) revealed that the "closed" arrangement with the binaphthol OH forming a hydrogen bond to the sulfonamide O-atom and only the triazolium H-atom activating the electrophile is energetically favored by about 15 kJ/mol. Thus, the less strained arrangement of the
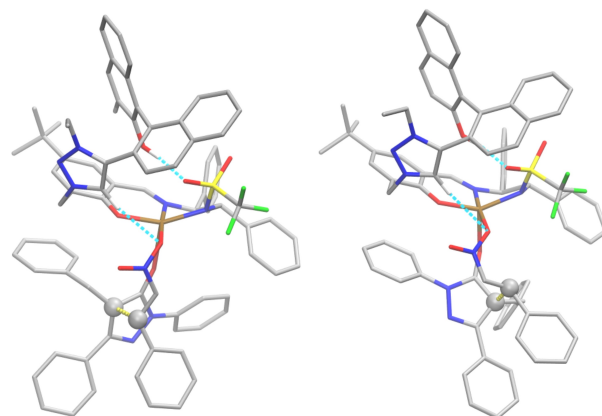

Figure 4. Comparison of the (4*S*,1′*S*)- (left) and the (4*S*,1′*R*)-transition states (right) for the C–C bond formation **I-2A** to **II**. Most H atoms are omitted for clarity, the C atoms involved in the C–C-bond formation are drawn as balls. Specific bond lengths are shown in Å, the bond to be formed is indicated by yellow dots. White: H, gray: C, brown: Cu, red: O, blue: N, yellow: S, green: F.
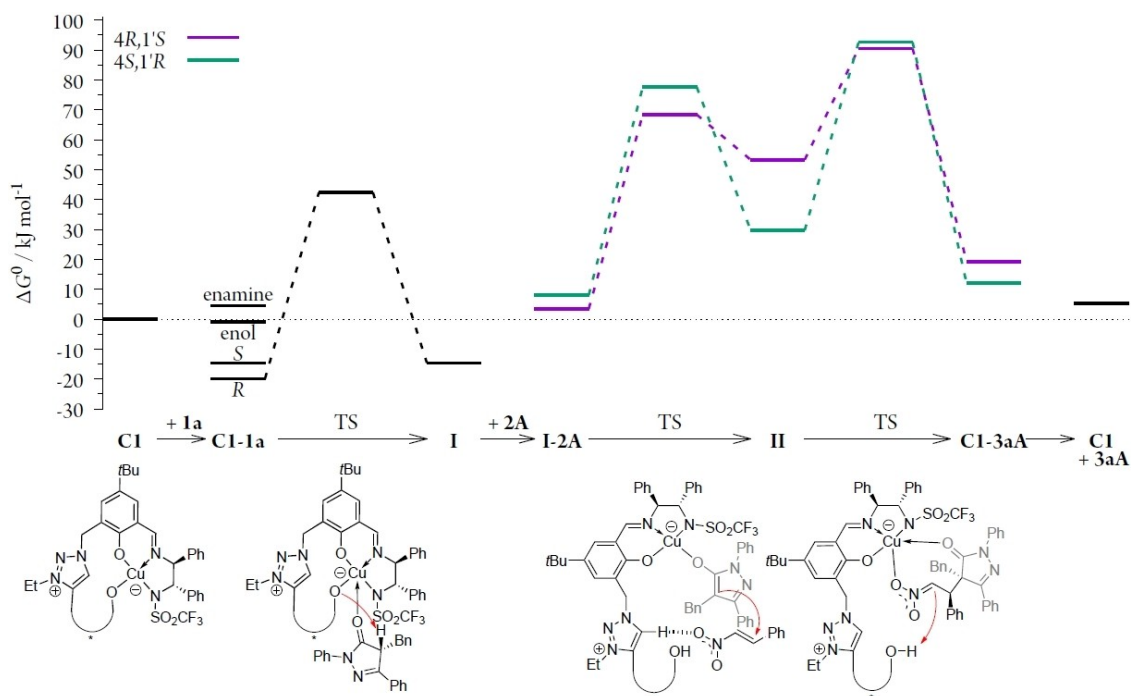
Figure 5. Free energy profile of the proposed catalytic cycle (see Scheme 5); purple curve for formation of the major enantiomer, green curve for the minor one. **C1** was chosen as reference state ($\Delta G^0 = 0.0$ kJ mol^{-1}). The data are summarized in Table S4.

Synthesis of Pyrazolidinones, β,γ'-Diaminoamides and further Derivatives

To use the 1,4-addition products for the synthesis of β,γ'-diaminoamides, a synthetic route was necessary featuring three chemoselective reductions (Scheme 6, *top*). In the first one the pyrazolone's imino group of **3bA** was reduced in 91 % yield by the borane-dimethylsulfide complex to give pyrazolidinone **7**. The reduction proceeded with very high diastereoselectivity, as—like in the starting material—only two diastereomers were detected with a dr of 94:6. The configuration of the newly formed stereocenter in **7** could be determined by X-ray crystal structure analysis (see Supporting Information).

DFT investigation of the reduction (Scheme S2 in the SI) predicts an energy profile shown in Figure S63 for the found diastereomer and in Figure S64 for its epimer. It turned out that the stereoselectivity of that reduction reaction is caused by steric interaction of the C(3) phenyl moiety with the two C(4) residues of the used pyrazalone (see Figure 6 and Figures S65 and S66). In the second chemoselective reduction the nitro group was transformed into the corresponding primary amine using zinc metal. Subsequently, the amine was protected by acylation to give pyrazolidinones **8**. Orthogonal protection of the protic pyrazolidinone N by a trifluoroacetyl group was followed by chemoselective reduction of the N,N-bond by SmI$_2$ to give the diaminoamide derivative **9**. Overall, this sequence proceeded with an overall yield of 68 %.

We also studied the removal of the PMP protecting group at N(1), which was readily achieved using cerium
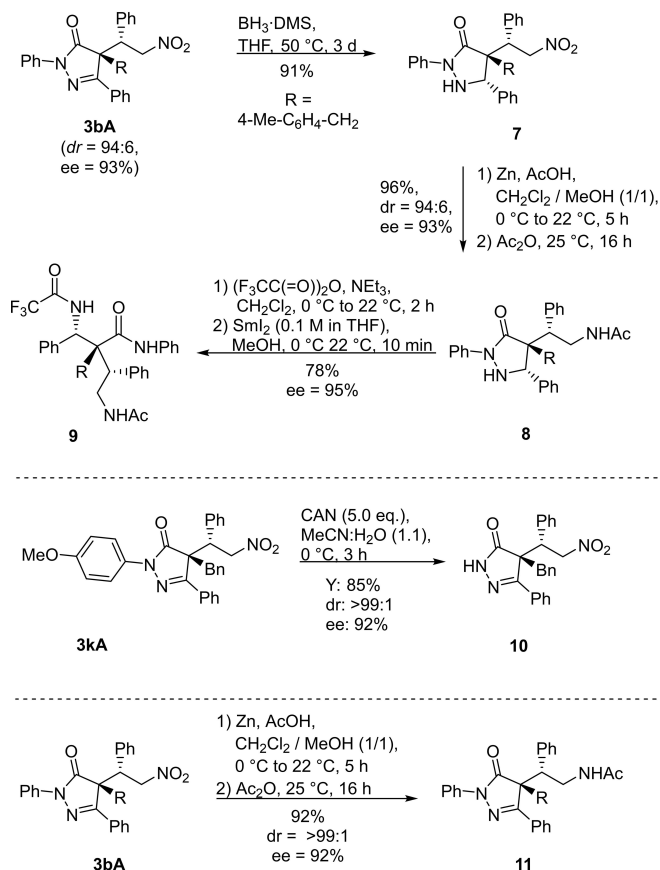
Scheme 6. Synthesis of β,γ'-diaminoamide **9** (top) and further pyrazolone derivatives (middle and bottom).
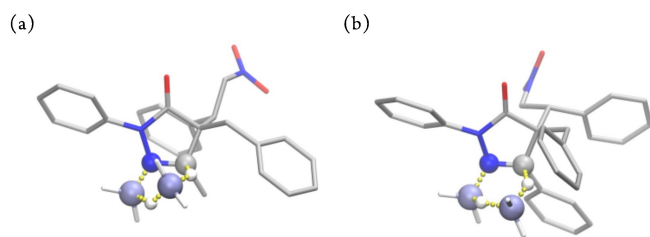
(a)   (b)

Figure 6. Comparison of the *R*- and *S*-transition states for the reduction of **3aA** (a: (*R*), b: (*S*)). Most H atoms are omitted for clarity, the atoms involved in the transition mode are drawn as balls, the bonds to be formed or broken are indicated by yellow dots. White: H, gray: C, red: O, blue: N, ice blue: B.

ammonium nitrate (CAN, $(NH_4)_2Ce(NO_3)_6$).[45] Moreover, we found that chemoselective reduction of the nitro group by zinc is also possible at the pyrazolone stage to give **11**. A crystal structure analysis confirmed the relative and absolute configuration of product **11** (see Figure 7).

Morphological Profiling

To detect bioactivity, the compound collection was explored using the Cell painting assay (CPA). CPA is a morphological profiling approach and allows detection of bioactivity in an unbiased manner (Figure 8)[46] U2OS cells were treated with the investigated compounds for 20 h prior to staining of DNA, mitochondria, endoplasmic reticulum, plasma membrane, Golgi, actin cytoskeleton, RNA and nucleoli. High-content imaging and analysis was performed and several hundred features were extracted and differences to the control (cells that were treated with DMSO) were expressed as Z scores. CPA profiles compile Z scores for 579 features.[47]

We use the percentage of significantly altered features (termed induction) to describe activity in CPA, and compounds with induction ≥ 5% are considered active. Similar profiles are expected to result from addressing the same target or mode of action (MoA). Profile similarity (termed biosimilarity) is employed to express similarity between profiles and two profiles are biosimilar for biosimilarity ≥ 75%. To generate target or MoA hypotheses, we profiled a set of 4251 reference compounds, i.e., small molecules with known targets or MoA and defined thus far twelve
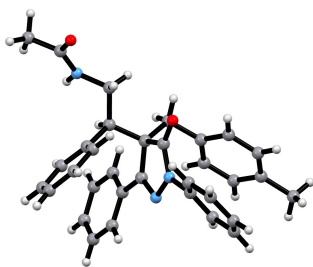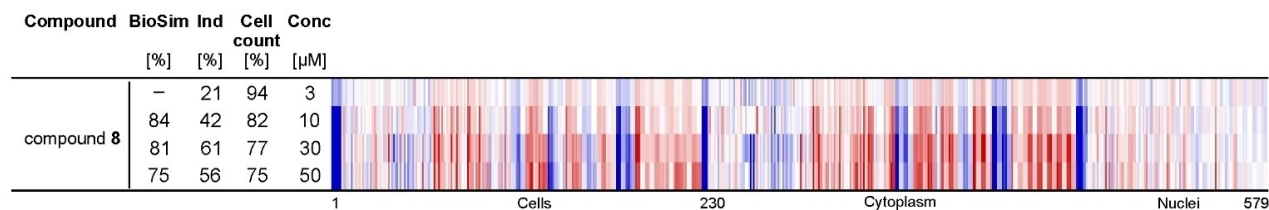

Figure 7. X-Ray crystal structure analysis of **11**.

bioactivity clusters that can be mapped using CPA.[48] Pyrazolone **11** was inactive up to 50 μM and diaminoamide **9** was weakly active at 50 μM (induction = 5.5%). In contrast, pyrazolone **3bA** and the pyrazolidinones **7** and **8** displayed activity already at 30, 10 and 3 μM, respectively (Figure 8). Compounds **3bA** and **7** were cytotoxic at 30 μM and 50 μM (cell count < 50%). For compound **8**, morphological changes are similar at different concentrations (Figure 8A) and mostly features related to area shape, ER (endoplasmatic reticulum) and DNA are altered (Figure S67). The biosimilarity to the twelve known bioactivity clusters was low except for the profile at 50 μM that displays some similarity to the BET (Bromodomain and Extra-Terminal motif) cluster (Figure 8B). In line with these data, the profiles of **8** localize close to the BET cluster in the lower dimension UMAP (Uniform Manifold Approximation and Projection) plot (Figure 8C and Figure S68A). However, as no BET inhibitors were among the most biosimilar reference compounds, **8** most likely does not target BET proteins. Compound **7** (10 μM) does not display high biosimilarity to the twelve bioactivity clusters (Figure 8D), however, localized close to the DNA synthesis cluster in the UMAP plot (Figure 8E and Figure S68B). 10 μM pyrazolidinone **7** showed the highest similarity to the DNA synthesis cluster (68%) and is biosimilar to Amsacrine and Campthotecin,[26] two topoisomerase I inhibitors that also share similarity with the DNA synthesis cluster. **7** mainly alters features that are related to the area shape and DNA (Figure S68C). The biosimilarity of **7** to the topoisomerase I inhibitors increase when only DNA-related features were considered (Figure 8F). The DNA synthesis cluster contains compounds with different targets. Pahl et al. recently demonstrated that the non-DNA cluster features can be used to separate the different mechanisms of action, e.g. Fe chelators, CDK (Cyclin-dependent kinase) inhibitors, nucleosides, antifolates and topoisomerase inhibitors.[48] Exploring the non-DNA cluster features assigned pyrazolidinone **7** to the topoisomerase I inhibitors (Figure S69), which strengthens the hypothesis for the putative mechanism of action.
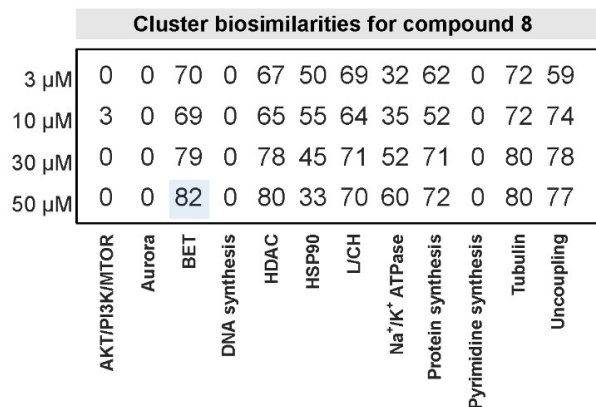
Conclusion

In summary, we have reported a highly enantio- and diastereoselective 1,4-addition of C(4)-substituted pyrazolones to nitroolefins. To achieve this, a new polyfunctional Cu^{II}-1,2,3-triazolium-aryloxide catalyst was developed offering a modus operandi that is reminiscent of enzymatic catalysis in various aspects. As extensive DFT studies show, the three key functional groups cooperate. The Lewis acid binds and acidifies the pronucleophile and the naphthoxide subsequently deprotonates the latter to form a reactive Cu-enolate. The naphthol OH generated in this event forms an intramolecular hydrogen bond with the sulfonamide part of the ligand to create a structurally well-defined supramolecular chiral cage as binding pocket, which is crucial for high stereocontrol in the subsequent 1,4-addition to the nitroolefin. The latter is shown to be activated by the
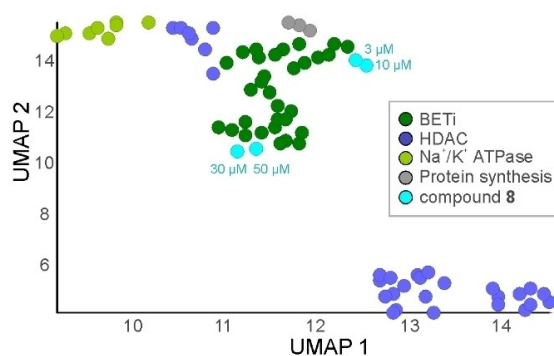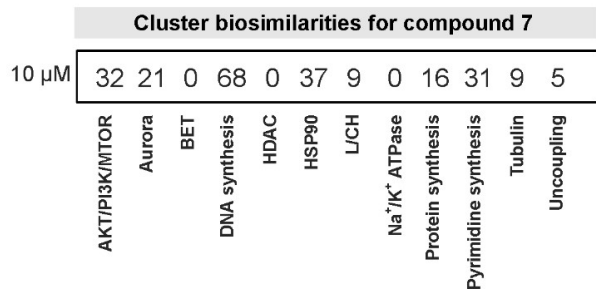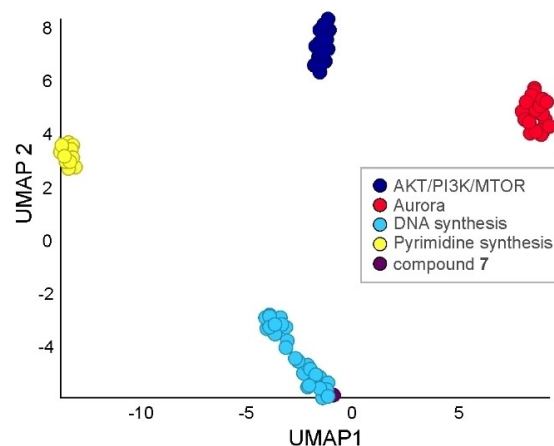
A

Compound	BioSim [%]	Ind [%]	Cell count [%]	Conc [µM]	
compound 8	–	21	94	3	
	84	42	82	10	
	81	61	77	30	
	75	56	75	50	

B

Cluster biosimilarities for compound 8

	AKT/PI3K/MTOR	Aurora	BET	DNA synthesis	HDAC	HSP90	L/CH	Na⁺/K⁺ ATPase	Protein synthesis	Pyrimidine synthesis	Tubulin	Uncoupling
3 µM	0	0	70	0	67	50	69	32	62	0	72	59
10 µM	3	0	69	0	65	55	64	35	52	0	72	74
30 µM	0	0	79	0	78	45	71	52	71	0	80	78
50 µM	0	0	82	0	80	33	70	60	72	0	80	77

C

D

Cluster biosimilarities for compound 7

	AKT/PI3K/MTOR	Aurora	BET	DNA synthesis	HDAC	HSP90	L/CH	Na⁺/K⁺ ATPase	Protein synthesis	Pyrimidine synthesis	Tubulin	Uncoupling
10 µM	32	21	0	68	0	37	9	0	16	31	9	5

E

F

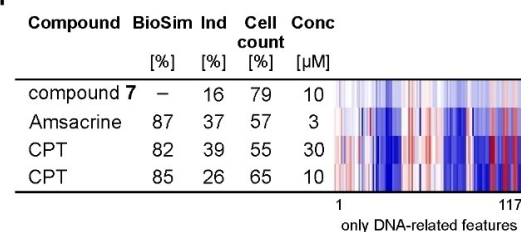| Compound	BioSim [%]	Ind [%]	Cell count [%]	Conc [µM]	
compound 7	–	16	79	10	
Amsacrine	87	37	57	3	
CPT	82	39	55	30	
CPT	85	26	65	10	

Figure 8. Cell painting detects bioactivity for compound **8** and **7**. (A–C) CPA profile analysis for compound **8**. (A) Profile comparison for compound **8** at 3, 10, 30 and 50 µM. The top line profile is set as a reference profile (100 % biological similarity, BioSim) to which the following profiles are compared. Blue color: decreased feature, red color: increased feature. (B) Cluster biosimilarity heatmap for **8**. (C) Localization of the CPA profiles for compound **8** in the lower dimension UMAP plot. Only the clusters with most similar features were included in the analysis. Not normalized data, 10 neighbors. See also Figure S67-A. (D–F) CPA profile analysis for compound **7**. (D) Cluster biosimilarity heatmap for compound **7**. (E) Localization of the CPA profiles for compound **7** in the lower dimension UMAP plot. Only the clusters with most similar features were included in the analysis. Not normalized data, 10 neighbors. (F) Profile comparison for compound **7** and the topoisomerase I inhibitors Amsacrine and Camptothecin (CPT). The top line profile is set as a reference profile (100 % biological similarity, BioSim) to which the following profiles are compared. Only DNA-related features were analyzed. See also Figure S68. Blue color: decreased feature, red color: increased feature. BioSim: biosimilarity, Ind: induction, Conc: concentration, L/CH: Lysosomotropism/cholesterol homeostasis.

1,2,3-triazolium moiety via single H-bond formation. Control experiments suggest that this activation is, like expected, considerably more efficient with 1,2,3-triazolium than with imidazolium. Moreover, the control experiments show the

vital role of the axial chirality of the triazolium/ naphthoxide unit to create an efficient chiral space. In addition, it is demonstrated that the densely functionalized addition products are valuable precursors for pyrazolidinones and β,γ'-diaminoamides, a previously unknown compound class, which was available via chemoselective C=N, nitro and N–N bond reductions. Morphological profiling identified biologically active compounds. In particular, pyrazolidone **7** shows biosimilarity to the anticancer lead structure Campto-thecin.

Acknowledgements

Conflict of Interest

The authors declare no conflict of interest.

Data Availability Statement

The data that support the findings of this study are available in the supplementary material of this article.

Keywords: 1,4-Additions · Confinement · Copper(II) · Density Functional Theory · Hydrogen Bonding

[1] a) Á. Mourelle-Insua, D. Méndez-Sánchez, J. L. Galman, I. Slabu, N. J. Turner, V. Gotor-Fernández, I. Lavandera, *Catal. Sci. Technol.* **2019**, *9*, 4083–4090; b) T. Le, P. Bérdi, I. Zupkó, F. Fülöp, Z. Szakonyi, *Int. J. Mol. Sci.* **2018**, *19*, 3522–3540.

[2] T. Mimoto, J. Imai, S. Tanaka, N. Hattori, O. Takahashi, Y. Kisanuki, Y. Nagano, M. Shintani, H. Hayashi, H. Sakikawa, K. Akaji, Y. Kiso, *Chem. Pharm. Bull.* **1991**, *39*, 2465–2467.

[3] D. Kim, L. Wang, M. Beconi, G. J. Eiermann, M. H. Fisher, H. He, G. J. Hickey, J. E. Kowalchick, B. Leiting, K. Lyons, F. Marsilio, M. E. McCann, R. A. Patel, A. Petrov, G. Scapin, S. B. Patel, R. S. Roy, J. K. Wu, M. J. Wyvratt, B. B. Zhang, L. Zhu, N. A. Thornberry, A. E. Weber, *J. Med. Chem.* **2005**, *48*, 141–151.

[4] a) Bestatin: H. Umezawa, T. Aoyagi, H. Suda, M. Hamada, T. Takeuchi, *J. Antibiot.* **1976**, *29*, 97–99; b) Lidocaine: J. P. Nolan, P. J. Baskett, in *Cambridge Textbook of Accident and Emergency Medicine* (Eds.: D. Skinner, A. Swain, R. Peyton, C. Robertson), Cambridge University Press, Cambridge, UK, p. 194.

[5] M. H. Paulsen, M. Engqvist, D. Ausbacher, N. B. Strøm, A. Bayer, *Org. Biomol. Chem.* **2016**, *14*, 7570–7578.

[6] a) J. L. Vicario, D. Badía, L. Carrillo, *J. Org. Chem.* **2001**, *66*, 9030–9032; b) S. Saito, T. Tsubogo, S. Kobayashi, *Chem. Commun.* **2007**, 1236–1237; c) L. Yin, L. Brewitz, N. Kumagai, M. Shibasaki, *J. Am. Chem. Soc.* **2014**, *136*, 17958–17961; d) L. Brewitz, F. A. Arteaga, L. Yin, K. Alagiri, N. Kumagai, M. Shibasaki, *J. Am. Chem. Soc.* **2015**, *137*, 15929–15939.

[7] D. Steinhuebel, Y. Sun, K. Matsumura, N. Sayo, T. Saito, *J. Am. Chem. Soc.* **2009**, *131*, 11316–11317.

[8] S. Qiao, J. Wu, J. Mo, P. Spigener, B. Zhao, B. Jiang, G. Li, *Synlett* **2017**, 2483–2488.

[9] J. Etxebarria, J. L. Vicario, D. Badia, L. Carrillo, N. Ruiz, *J. Org. Chem.* **2005**, *70*, 8790–8800.

[10] a) D.-Y. Ma, D.-X. Wang, J. Pan, Z.-T. Huang, M.-X. Wang, *J. Org. Chem.* **2008**, *73*, 4087–4091; b) X.-G. Li, M. Lähitie, L. T. Kanerva, *Tetrahedron: Asymmetry* **2008**, *19*, 1857–1861; c) T. Heck, D. Seebach, S. Osswald, M. K. J. ter Wiel, H.-P. E. Kohler, B. Geueke, *ChemBioChem* **2009**, *10*, 1558–1561.

[11] N. Wannenmacher, M. Heberle, X. Yu, A. Demircan, D. M. Wanner, C. Pfeffer, R. Peters, *Adv. Synth. Catal.* **2022**, *364*, 3396–3403.

[12] a) K. Brune, *Acute Pain* **1997**, *1*, 33–40; b) P. Gupta, J. K. Gupta, S. Bansal, A. K. Halve, *Int. J. Curr. Pharm. Res.* **2015**, *7*, 25–29.

[13] a) H. Yoshida, H. Yanai, Y. Namiki, K. Fukatsu-Sasaki, N. Furutani, N. Tada, *CNS Drug Rev.* **2006**, *12*, 9–20; b) P. Gupta, J. K. Gupta, A. K. Halve, *Int. J. Pharm. Sci. Res.* **2015**, *6*, 2291–2310; c) G. Varvounis, in *Advances in Heterocyclic Chemistry*, Academic Press, New York, **2009**, pp. 143–224.

[14] R. N. Brogden, *Drugs* **1986**, *32*, 60–70.

[15] M. S. Chande, P. A. Barve, V. Suryanarayan, *J. Heterocycl. Chem.* **2007**, *44*, 49–53.

[16] a) M. P. Clark, S. K. Laughlin, M. J. Laufersweiler, R. G. Bookland, T. A. Brugel, A. Golebiowski, M. P. Sabat, J. A. Townes, J. C. VanRens, J. F. Djung, M. G. Natchus, B. De, L. C. Hsieh, S. C. Xu, R. L. Walter, M. J. Mekel, S. A. Heitmeyer, K. K. Brown, K. Juergens, Y. O. Taiwo, M. J. Janusz, *J. Med. Chem.* **2004**, *47*, 2724–2727; b) C. Pargellis, J. Regan, *Curr. Opin. Invest. Drugs* **2003**, *4*, 566–571.

[17] K. Abe, Y. Itoyama, G. Sobue, S. Tsuji, M. Aoki, M. Doyu, C. Hamada, K. Kondo, T. Yoneoka, M. Akimoto, H. Yoshino, *Amyotrophic Lateral Scler. Frontotemporal Degener.* **2014**, *15*, 610–617.

[18] a) S. Yoon, B. Choi, M. M. Rahman, S. Kumar, S. M. Mamun Kabir, J. Koh, *Materials* **2019**, *12*, 4209; b) F. Karcı, F. Karcı, *Dyes Pigm.* **2008**, *76*, 147–157; c) J. S. Casas, M. S. García-Tasende, A. Sánchez, J. Sordo, Á. Touceda, *Coord. Chem. Rev.* **2007**, *251*, 1561–1589; d) J. Bao, C. Tang, R. Tang, *J. Rare Earth* **2011**, *29*, 15–19.

[19] a) X. Bao, X. Wang, J.-M. Tian, X. Ye, B. Wang, H. Wang, *Org. Biomol. Chem.* **2022**, *20*, 2370–2386; b) P. Chauhan, S.

Mahajan, D. Enders, *Chem. Commun.* **2015**, *51*, 12890–12907; c) C. Bailly, P.-E. Hecquet, M. Kouach, X. Thuru, J.-F. Goossens, *Bioorg. Med. Chem.* **2020**, *28*, 115463.

[20] S. Liu, X. Bao, B. Wang, *Chem. Commun.* **2018**, *54*, 11515–11529.

[21] Y.-H. Liao, W.-B. Chen, Z.-J. Wu, X.-L. Du, L.-F. Cun, X.-M. Zhang, W.-C. Yuan, *Adv. Synth. Catal.* **2010**, *352*, 827–832.

[22] Another non-diastereoselective reaction with moderate ee has reported: C. Wang, X. Yang, D. Enders, *Chem. Eur. J.* **2012**, *18*, 4832–4835.

[23] T. Okino, Y. Hoashi, Y. Takemoto, *J. Am. Chem. Soc.* **2003**, *125*, 12672–12673.

[24] a) J.-H. Li, D.-M. Du, *Org. Biomol. Chem.* **2013**, *11*, 6215–6223; b) J. H. Li, D. M. Du, *Org. Biomol. Chem.* **2015**, *13*, 5636–5645; c) K. S. Rao, P. Ramesh, R. Trivedi, M. L. Kantam, *Tetrahedron Lett.* **2016**, *57*, 1227–1231; d) Y. H. Kim, J. H. Yoon, M. Y. Lee, D. Y. Kim, *Bull. Korean Chem. Soc.* **2017**, *38*, 1242–1245; e) Z. Wang, S. Ban, M. Yang, Q. Li, *ChemistrySelect* **2017**, *2*, 3419–3422.

[25] Ooi et al. studied chiral ammonium/ aryloxide zwitterions in organocatalysis. For a review, see: D. Uraguchi, T. Ooi, *J. Synth. Org. Chem. Jpn.* **2018**, *76*, 1144–1153.

[26] a) M. E. Wall, in *Chronicles of Drug Discovery* (Ed.: D. Lednicer,), American Chemical Society, Washington, D. C. **1993**, pp. 327–348; b) C. J. Thomas, N. J. Rahier, S. M. Hecht, *Bioorg. Med. Chem.* **2004**, *12*, 1585–1604; c) R. Peters, M. Althaus, A.-L. Nagy, *Org. Biomol. Chem.* **2006**, *4*, 498–509; d) R. Peters, M. Althaus, C. Diolez, A. Rolland, E. Manginot, M. Veyrat, *J. Org. Chem.* **2006**, *71*, 7583–7595.

[27] F. Willig, J. Lang, A. C. Hans, M. R. Ringenberg, D. Pfeffer, W. Frey, R. Peters, *J. Am. Chem. Soc.* **2019**, *141*, 12029–12043.

[28] V. Miskov-Pajic, F. Willig, D. M. Wanner, W. Frey, R. Peters, *Angew. Chem. Int. Ed.* **2020**, *59*, 19873–19877.

[29] a) B. Schulze, U. S. Schubert, *Chem. Soc. Rev.* **2014**, *43*, 2522–2571; b) J. Cai, J. L. Sessler, *Chem. Soc. Rev.* **2014**, *43*, 6198–6213.

[30] Overview of hydrogen bonds in cooperative catalysis: X. Lu, L. Deng, in *Cooperative Catalysis – Designing Efficient Catalysts for Synthesis* (Ed.: R. Peters), Wiley-VCH, Weinheim, **2015**.

[31] For a review of related concepts, see X. Ye, C.-H. Tan, *Chem. Sci.* **2021**, *12*, 533–539.

[32] For triazoliums as organocatalysts, see e.g. K. Ohmatsu, M. Kiyokawa, T. Ooi, *J. Am. Chem. Soc.* **2011**, *133*, 1307–1309.

[33] a) J. Schmid, T. Junge, J. Lang, W. Frey, R. Peters, *Angew. Chem. Int. Ed.* **2019**, *58*, 5447–5451; for pioneering work, see: b) H. C. Kolb, M. G. Finn, B. Sharpless, *Angew. Chem. Int. Ed.* **2001**, *40*, 2004–2021; c) V. V. Rostovtsev, L. G. Green, V. V. Fokin, B. A. Sharpless, *Angew. Chem. Int. Ed.* **2002**, *41*, 2596–2599.

[34] H. Yang, J. L. Peterseny, K. K. Wang, *Tetrahedron* **2006**, *62*, 8133–8141.

[35] Deposition numbers 2195835 (for **6**), 2195838 (for **7**), 2253655 (for **L1-Br**) and 2195836 (for **11**) contain the supplementary crystallographic data for this paper. These data are provided free of charge by the joint Cambridge Crystallographic Data Centre and Fachinformationszentrum Karlsruhe Access Structures service.

[36] Ma et al. reported a sequence consisting of an initial 1,4-addition and a subsequent fluorination step: F. Li, L. Sun, Y. Teng, P. Yu, J. C.-G. Zhao, J.-A. Ma, *Chem. Eur. J.* **2012**, *18*, 14255–14260.

[37] For pioneering work on the general concept of cooperative Lewis acid/Brønsted base catalysis, see e.g.: a) M. Shibasaki, N. Kumagai, *Lewis acid-Brønsted base catalysis, in Cooperative Catalysis – Designing Efficient Catalysts for Synthesis* (Ed.: R. Peters), Wiley-VCH, Weinheim, **2015**; b) M. Shibasaki, N. Yoshikawa, *Chem. Rev.* **2002**, *102*, 2187; c) H. Sasai, T. Suzuki, S. Arai, T. Arai, M. Shibasaki, *J. Am. Chem. Soc.* **1992**, *114*, 4418; d) H. Sasai, T. Arai, Y. Satow, K. N. Houk, M. Shibasaki, *J. Am. Chem. Soc.* **1995**, *117*, 6194; e) M. Tokunaga, J. F. Larrow, F. Kakiuchi, E. N. Jacobsen, *Science* **1997**, *277*, 936; f) J. M. Ready, E. N. Jacobsen, *J. Am. Chem. Soc.* **1999**, *121*, 6086.

[38] T. Satyanarayana, S. Abraham, H. B. Kagan, *Angew. Chem. Int. Ed.* **2009**, *48*, 456–494.

[39] J. Peisach, W. E. Blumberg, *Arch. Biochem. Biophys.* **1974**, *165*, 691–708.

[40] a) P. J. Benites, D. S. Rawat, J. M. Zaleski, *J. Am. Chem. Soc.* **2000**, *122*, 7208–7217.

[41] A. C. Hans, P. M. Becker, J. Haußmann, S. Suhr, D. M. Wanner, V. Lederer, F. Willig, W. Frey, B. Sarkar, J. Kästner, R. Peters, *Angew. Chem. Int. Ed.* **2023**, *62*, e202217519.

[42] J. Schmid, W. Frey, R. Peters, *Organometallics* **2017**, *36*, 4313–4324.

[43] While an exergonic overall reaction is expected, we obtained, in the calculations, a slightly positive ΔG^0 of 5.3 kJ mol^{-1}. That is within the expected error and may be caused by deficiencies in the computational description of the solvation or the estimation of the entropy (see Supporting Information).

[44] DFT calculations: a) B.-L. Li, Y.-F. Wang, S.-P. Luo, A.-G. Zhong, Z.-B. Li, X.-H. Du, D.-Q. Xu, *Eur. J. Org. Chem.* **2010**, 656–662; review: b) A. M. F. Phillips, M. H. G. Prechtl, A. J. L. Pombeiro, *Catalysts* **2021**, *11*, 569.

[45] G. Onodera, T. Toeda, N. N. Toda, D. Shibagishi, R. Takeuchi, *Tetrahedron* **2010**, *66*, 9021–9031.

[46] a) M. A. Bray, S. Singh, H. Han, C. T. Davies, B. Borgeson, C. Hatland, M. Kost-Alimova, S. M. Gustafsdottir, C. C. Gibson, A. E. Carpenter, *Nat. Protoc.* **2016**, *11*, 1757–1774; b) S. M. Gustafsdottir, V. Ljosa, K. L. Sokolnicki, J. A. Wilson, D. Walpita, M. M. Kemp, K. Petri Seiler, H. A. Carrel, T. R. Golub, S. L. Schreiber, P. A. Clemons, A. E. Carpenter, A. F. Shamji, *PLoS One* **2013**, *8*, e80999.

[47] A. Christoforow, J. Wilke, A. Binici, A. Pahl, C. Ostermann, S. Sievers, H. Waldmann, *Angew. Chem. Int. Ed.* **2019**, *58*, 14715–14723.

[48] A. Pahl, B. Schölermann, M. Rusch, M. Dow, C. Hedberg, A. Nelson, S. Sievers, H. Waldmann, S. Ziegler, *bioRxiv preprint* **2022**, https://doi.org/10.1101/2022.08.15.503944.